Behaviour of U(VI) solids under conditions of natural aquatic systems

G. Meinrath and T. Kimura

Department of Chemistry, Analytical Chemistry Division, Japan Atomic Energy Research Institute, Tokai-mura, Ibaraki 319 (Japan)

(Received June 15, 1992; revised September 11, 1992)

Abstract

Solid–liquid equilibria of U(VI) under 100, 0.98 and 0.03% CO_2 partial pressures were studied in the pH range 2.8–4.6 in 0.1 M $NaClO_4$ solution at 24±2 °C. UO_2CO_3 and $UO_3 \cdot 2H_2O$ are found as solubility limiting solid phases with lg $K_{sp}(UO_2CO_3) = -13.89 \pm 0.11$ and lg $K_{sp}(UO_3 \cdot 2H_2O) = -22.28 \pm 0.19$. Furthermore, free energies of formation were calculated to be $\Delta G°_f(UO_2CO_3) = -1562.2 \pm 3.3$ kJ mol^{-1} and $\Delta G°_f(UO_3 \cdot 2H_2O) = -1633.3 \pm 3.5$ kJ mol^{-1}.

Introduction

Solubility products of $UO_2CO_3(s)$ have been determined in 0.02 M ($NaHCO_3$/HCl/$HClO_4$) solutions under pure CO_2 atmosphere in the temperature range 25–200 °C [1] and in 0.5 and 3.0 M $NaClO_4$ at 25 °C in equilibrium with nitrogen/CO_2 mixtures containing 4.8–98% CO_2 [2].

$UO_2(OH)_2$ [3–5], $UO_3 \cdot H_2O$ [6] and $UO_3 \cdot 2H_2O$ [7] are given as equilibrium solid phases in 0.1 M $NaNO_3$ solutions under CO_2 free nitrogen [3], at variable ionic strength in HNO_3/NH_3 solutions [4], in 0.2 M NH_4NO_3 solutions [5], at variable ionic strength in $HClO_4$ and NaOH solutions under nitrogen [6] and in 0.5 M $HClO_4$ solutions at 25 °C under nitrogen atmosphere [7].

Natural aquatic systems are known to have CO_2 partial pressures in the range 0.03–10% [8]. Most of the hitherto known data has either been determined under nitrogen [3, 6, 7] or at elevated CO_2 partial pressures $\geq$4.8%. Therefore, no experimental data is available on solid–liquid equilibria of U(VI) under conditions of natural aquatic systems, e.g. partial pressures slightly higher than the CO_2 partial pressure of air, that is 0.03%.

The present experiments have been done under 100, 0.98 and 0.03% CO_2 partial pressures (i) to obtain reliable information on the relevant solid phases under conditions of natural aquatic systems, (ii) to obtain solubility products of these solid phases and (iii) to determine the stability region of these solid phases with respect to CO_2 partial pressure.

Experimental

Solubility experiments were conducted as pH titrations in glass vessels of 200 ml volume in the pH range 2.8–4.6 in equilibrium with pure CO_2, nitrogen/0.98% CO_2 (Nihon Sanso Co.) or air. The gas mixtures were bubbled through the solutions continuously after moistening in washing flasks. The ionic strength of the solutions was adjusted by 0.1 M $NaClO_4$. Temperature is 24±2 °C. The solid phases were precipitated from about 2×10^{-3} M U(VI) solutions by addition of 0.05 M Na_2CO_3. The systems were left to equilibrate for three weeks. pH titrations were made by addition of either 0.1 M NaOH, 0.05 M Na_2CO_3 or 0.1 M $HClO_4$. pH was measured simultaneously by two glass electrodes (ROSS-type, Orion Co.) after calibration with standard buffer solutions. The quality of the pH measurements has further been checked by reproducing previous results [9, 10]. U(VI) concentrations were determined by UV–Vis spectroscopy using Beer's law. The spectrometer (Kyowa Co.) was calibrated by UO_2^{2+} solutions of known concentration. Phase separations were made by ultrafiltration at 0.45 or 0.2 μm pore size. No hint on colloidal species could be found by ultrafiltration studies through 0.8 μm to 1.3 nm pore size. Solid phases were characterized by differential thermal analysis (DTA) and thermogravimetry (TGA) (Shimadzu Co.), photoacoustic FTIR spectroscopy (FTIR-PAS) (Jasco Co.), solid phase UV–Vis photoacoustic spectroscopy (PAS) (Jasco Co.) and X-ray crystallography (Rigaku Co.). DTA/TGA is made simultaneously. The

0020-1693/93/$6.00

air-dried samples (15–25 mg) were heated up and cooled down by a heating/cooling rate of 10 K min^{-1} in the temperature range 25–1000 °C in air.

Details on FTIR-PAS and PAS equipment are given elsewhere [11].

Results and discussion

Physicochemical state of solid phases

The solid phase formed under 100% CO_2 partial pressure was found as a faint yellow-greenish powder. The X-ray diffraction data of this solid is compared to literature data known for UO_2CO_3 (rutherfordine) [12] in Table 1.

DTA/TGA shows a single distinct endothermic signal at 600 °C due to loss of CO_2. A broad weak signal in the temperature range 60–160 °C indicated release of water. It is interpreted as adsorbed water with an amount of 0.6–0.9 formula units. The final product is crystalline U_3O_8, identified by its X-ray pattern [13]. The experimentally determined weight loss is in agreement with the composition $UO_2CO_3 \cdot (0.6–0.9)H_2O$. The FTIR-PA spectrum of this phase is given in Fig. 1(a) and summarized in Table 2.

The solids formed under 0.98 and 0.03% CO_2 partial pressures were found as bright yellow powders. The X-ray diffraction pattern of these phases is given in Fig. 2 and compared to literature data for $UO_3 \cdot 2H_2O$ [14] in Table 1.

DTA/TGA analysis showed a strong endothermic signal at 110 °C due to loss of water. At 260–320 °C, the formation of an intermediate compound $UO_3 \cdot 0.5H_2O$ was indicated by DTA and TGA, followed by a continuous weight loss up to 1000 °C. The sample's weight increased slightly when cooled down slowly. U_3O_8(cr) was found as the final product. The weight changes were found in agreement with the composition $UO_3 \cdot (2–2.2)H_2O$. FTIR-PA spectra are given in Fig. 1(b) and (c), respectively, and summarized in Table 2. The IR bands are fairly weak. A contamination with carbonate is indicated in Fig. 1(b) and (c). It is found

TABLE 1. Comparison of X-ray data for the solids precipitated under 100, 0.98 and 0.03% CO_2 partial pressures with data available in the literature (*d* values in pm)

100% CO_2	UO_2CO_3 [12]	0.98%/0.03% CO_2	$UO_3 \cdot 2H_2O$ [14]
465	461	741	737
431	430	635	664
389	392	459	
321	323	369	369
264	264	360	359
260.8	260	352	352
250.4	251.2	336	
243.1	242.0	324	323
231.8	230.9	318	317
215.3	215.6	299	298.5
205.9	206.2	272	278
193.9	195.3	257	258/255
191.3	192.6	230	228/226
187.8	187.9	209	209
174.3	174.6	205	206
	172.3	200	200
170.0	170.1	197	198

All lines with relative intensities ⩾ 5 are shown by the precipitated phases. Additional lines in the solids at 0.98%/0.03% CO_2 partial pressure can be explained as 459 pm = [3 1 0] and 336 pm = [0 5 0; 0 2 3] [*hkl*] in the orthorhombic crystal system given in ref. 14.

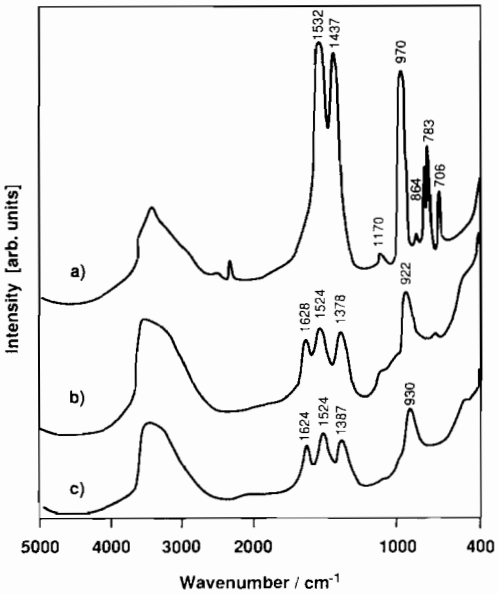

Fig. 1. FTIR-PA spectra of the solids formed under 100% (a), 0.98% (b) and 0.03% (c) CO_2 partial pressures.

TABLE 2. Interpretation of IR absorption bands in the solid phases precipitated under 100, 0.98 and 0.03% CO_2 partial pressures (in cm^{-1})

100% CO_2	0.98%/0.03% CO_2	Assignment	Reference
706		CO_3 (ν_5)	16
783		CO_3 (ν_3)	16
864		UO_2 sym.	17
970	930/922	UO_2 as.	17
1170		UO_2 as. + bend.	17
1437	1380[a]	CO_3 (ν_1)	16
1532	1520[a]	CO_3 (ν_4)	16
	1624	H_2O bend.	18
3600	3600	H_2O strech.	18

[a]These lines are also interpreted as combination overtones of the uranyl group (cf. ref. 15). sym.: symmetric fundamental vibration; as.: asymmetric fundamental vibration; bend.: bending vibration; strech.: stretching vibration.

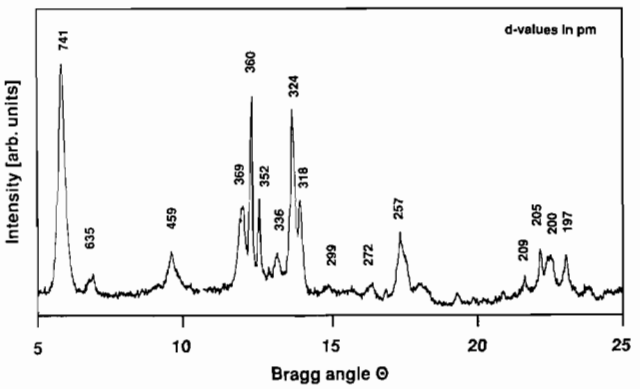

Fig. 2. X-ray diffraction pattern of the solids formed under 0.98 and 0.03% CO_2 partial pressures.

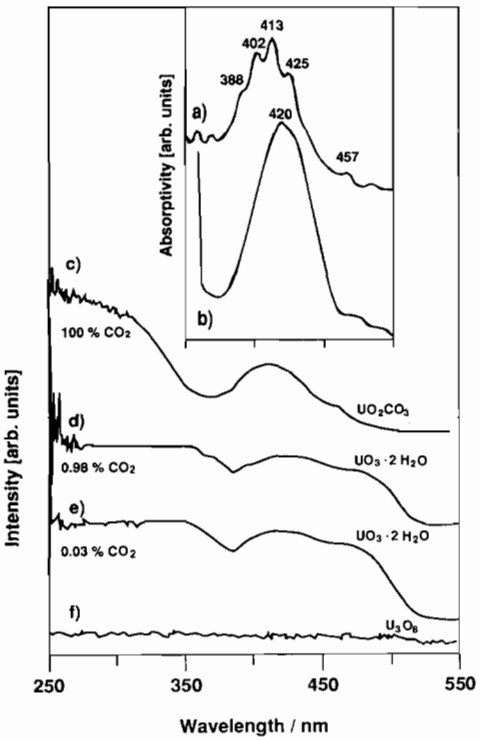

Fig. 3. UV–Vis spectra of U(VI) under 100% (a) and 0.98%/0.03% (b) CO_2 partial pressures. PA spectra of the U(VI) solids formed under 100% (c), 0.98% (d) and 0.03% (e) CO_2 partial pressures. (f) PA spectrum of $U_3O_{8(cr)}$.

to be beyond the analytical limits of the DTA/TGA equipment and interpreted as coprecipitated material. The solid phases did not contain hydroxyl, as indicated by the absence of the hydroxyl group stretching vibration band at about 3450 cm^{-1} [19].

In Fig. 3(c)–(e) the UV–Vis-PA spectra of the equilibrium solid phases under the investigated CO_2 partial pressures are shown. The PA spectrum of UO_2CO_3 gives a broad signal in the range 370–500 nm, with the same maximum as the UV–Vis spectrum of the free ion in solution (cf. Fig. 3(a)). The resolution of the PA spectrometer is 16 nm and consequently the fine structure of the band, if any, could not be resolved.

The PA spectra of $UO_3 \cdot 2H_2O$ (Fig. 3(d) and (e)) at wavelengths above 370 nm show a broader absorption band with a saddle point at about 450 nm. The maxima at the left side of the saddle point were found in the same range as the free ion's absorption (cf. Fig. 3(a)), whereas the right side maxima lie outside the free ion's absorption range. In Fig. 3(f), the PA spectrum of U_3O_8 is given to illustrate that a uranyl solid phase does not necessarily have a characteristic PA spectrum. The spectrum of U_3O_8 is featureless, in agreement with the literature [20].

Analysis of the U(VI) solid phases indicates the formation of crystalline UO_2CO_3 (rutherfordine) under 100% CO_2 partial pressure and less crystalline $UO_3 \cdot 2H_2O$ (schoepite) under both 0.98 and 0.03% CO_2 partial pressures.

Solubility studies

The solubility product of $UO_2CO_3(s)$ is given by

$$\lg K_{sp}(UO_2CO_3) = \lg[UO_2^{2+}] + \lg[CO_3^{2-}] \quad (1)$$

The solubility product of $UO_3 \cdot 2H_2O(s)$ (abbreviated as UO_3) is given by

$$\lg K_{sp}(UO_3) = \lg[UO_2^{2+}] + 2\lg[OH^-] \quad (2)$$

Hydroxide concentrations are calculated from measured pH and the ionic product of water K_w in 0.1 M $NaClO_4$ solution by

$$\lg[OH^-] = \lg K_w + pH \quad (3)$$

with $\lg K_w = -13.78 \pm 0.01$ [21].

Carbonate concentrations are calculated from measured pH by the Henry constant K_H and the dissociation constants K^*, K' and K_2 of CO_2 in 0.1 M $NaClO_4$

$$CO_{2(g)} \overset{K_H}{\longleftrightarrow} CO_{2(aq)} \overset{K^*}{\longleftrightarrow} H_2CO_3 \overset{K'}{\longleftrightarrow} HCO_3^- + H^+ \overset{K_2}{\longleftrightarrow} CO_3^{2-} + 2H^+ \quad (4)$$

The value $\Sigma\lg K = \lg(K_H K^* K' K_2)$ has been determined to be $\Sigma\lg K = -17.62 \pm 0.07$ [22].

Carbonate concentrations are calculated from eqn. (5)

$$\lg[CO_3^{2-}] = \Sigma\lg K + \lg p_{CO_2} + 2pH \quad (5)$$

where p_{CO_2} is the CO_2 partial pressure in atm and $\Sigma\lg K = -17.62 \pm 0.07$.

For UO_2^{2+} concentrations in equilibrium with $UO_2CO_3(s)$ eqn. (6) follows from eqn. (1)

$$\lg[UO_2^{2+}] = \lg K_{sp}(UO_2CO_3) - \lg[CO_3^{2-}] \quad (6)$$

Combination of eqns. (1) and (5) gives

$$\lg[UO_2^{2+}] = \lg K_{sp}(UO_2CO_3) - \Sigma\lg K - \lg p_{CO_2} - 2pH \quad (7)$$

Similarly, from eqns. (2) and (5), eqn. (8) follows for equilibria with $UO_3 \cdot 2H_2O(s)$

$$\lg[UO_2^{2+}] = \lg K_{sp}(UO_3) - 2\lg K_w + \Sigma\lg K + \lg p_{CO_2} - \lg[CO_3^{2-}] \quad (8)$$

and by combining eqns. (2) and (3)

$$\lg[UO_2^{2+}] = \lg K_{sp}(UO_3) - 2\lg K_w - 2pH \quad (9)$$

Equation (9) suggests, that for solid–solid equilibria of $UO_3 \cdot 2H_2O(s)$, $\lg[UO_2^{2+}]$ is a linear function of pH with a slope of -2, irrespective of p_{CO_2}. In the case of $UO_2CO_3(s)$, eqn. (7) suggests that $\lg[UO_2^{2+}]$ is a linear function of pH only at constant p_{CO_2}.

Interpretations of experimental results by eqns. (7) and (9) are given in Fig. 4, illustrating linear correlations of lg[U(VI)] with pH of slope -2. The experimental data determined at 0.98 and 0.03% CO_2 partial pressure shows the same linear correlation independent of p_{CO_2}. This is in agreement with eqn. (9) since the solid involved in the equilibrium is $UO_3 \cdot 2H_2O(s)$. The data obtained in equilibrium with $UO_2CO_3(s)$ under 100% CO_2 partial pressure correlates with a separate line of slope -2. As indicated by eqn. (7) this equilibrium further depends on p_{CO_2}.

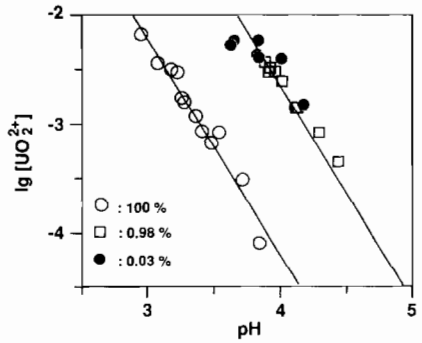

Fig. 4. Equilibrium concentrations $\lg[UO_2^{2+}]$ as function of pH.

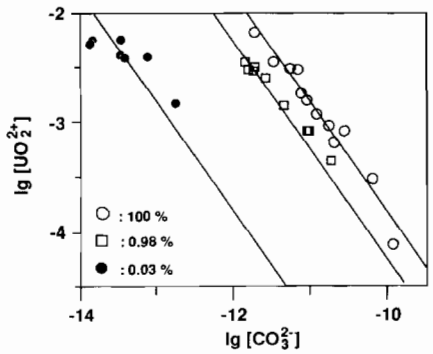

Fig. 5. Equilibrium concentrations $\lg[UO_2^{2+}]$ as function of $\lg[CO_3^{2-}]$.

Equations (6) and (8) explain that, as function of $\lg[CO_3^{2-}]$, $\lg[UO_2^{2+}]$ is a linear function of p_{CO_2} only in equilibrium with $UO_2CO_3(s)$, whereas in equilibria with $UO_3 \cdot 2H_2O(s)$, $\lg[UO_2^{2+}]$ is a linear function of slope -1 only at constant p_{CO_2}. This is shown in Fig. 5. The experimental points are found to be scattered around lines with slope -1, separate for each p_{CO_2}.

The solubility data given in Figs. 4 and 5 have been measured from both undersaturation and supersaturation. Steady state was reached within 2–3 days in equilibrium with $UO_2CO_3(s)$ and 7–14 days in equilibrium with $UO_3 \cdot 2H_2O(s)$.

Spectroscopic investigation

UV–Vis spectroscopy is used to investigate the state of U(VI) in the aqueous solutions. Figure 3(a) gives the spectrum of the free $UO_2^{2+}{}_{(aq)}$ ion [23], as found under 100% CO_2 partial pressure in the pH range 2.4–4. The UV–Vis spectrum of U(VI) in solutions under 0.98 and 0.03% CO_2 partial pressures in the pH range 3.5–4.5 is given in Fig. 3(b). It is quite different from the spectrum of $UO_2^{2+}{}_{(aq)}$. Its intensity in the absorption maximum at 420.2 nm is about four times that of the $UO_2^{2+}{}_{(aq)}$ ion measured after acidification. It indicates the presence of complexed U(VI) species. The absorption ratio of a hydrolyzed solution and the same solution after acidification remained unchanged in the investigated pH range 3.5–4.6. A theoretical analysis, based on currently available data on the hydrolysis and carbonate complexation of U(VI) [24], indicated, that neither $(UO_2)_3(OH)_4^{2+}$ nor $(UO_2)_3(OH)_5^{+}$ or $UO_2CO_3^0$ should play any role in the investigated pH region. Recent data [25] indicates, that the UO_2OH^+ and the $UO_2(OH)_2^0$ species must be taken into account only at pH values >4.6. The only complexed species playing a role in the investigated pH range is found to be the dimeric $(UO_2)_2(OH)_2^{2+}$ species. The concentration of the dimer $(UO_2)_2(OH)_2^{2+}$ is given by eqn. (10)

$$\lg[(UO_2)_2(OH)_2^{2+}] = \lg \beta_{22} + 2\lg[UO_2^{2+}] + 2\lg[OH^-] \quad (10)$$

In equilibrium with $UO_3 \cdot 2H_2O(s)$, $\lg[UO_2^{2+}]$ can be expressed by eqn. (9), resulting in

$$\lg[(UO_2)_2(OH)_2^{2+}] = \lg \beta_{22} + 2\lg K_{sp}(UO_3) - 2\lg K_w - 2pH \quad (11)$$

Comparison of eqns. (9) and (11) shows that in equilibrium with the solid phase $UO_3 \cdot 2H_2O(s)$ both $\lg[(UO_2)_2(OH)_2^{2+}]$ and $\lg[UO_2^{2+}]$ decrease parallel

with a slope of -2 with pH. The concentration ratio is given by eqn. (12) and independent of pH

$$R = \lg([(UO_2)_2(OH)_2^{2+}]/[UO_2^{2+}])/$$
$$= \lg K_{sp}(UO_3) + \lg \beta_{22} \quad (12)$$

The experimental data on the formation constant lg K_{22} in 0.1 M solution at 25 °C which are available in the literature are summarized in Table 3. To correct for the formation of the dimer, the data in Table 3 are averaged, excluding the somewhat small value of ref. 31. A value of lg $K_{22} = -5.97 \pm 0.16$ is obtained. Combination with eqn. (3) gives lg $\beta_{22} = 21.59 \pm 0.18$.

Interpreting our data with lg $\beta_{22} = 21.59 \pm 0.18$, the solubility products

100%: lg $K_{sp}(UO_2CO_3) = -13.89 \pm 0.11$
0.98%: lg $K_{sp}(UO_3) = -22.20 \pm 0.12$
0.03%: lg $K_{sp}(UO_3) = -22.34 \pm 0.23$
0.98% + 0.03%: lg $K_{sp}(UO_3) = -22.28 \pm 0.19$

and $R = -0.69 \pm 0.37$, corresponding to about 10–40% of the dimer, are evaluated.

The results of this study are summarized in Fig. 6. From the experimentally determined solubility products, $lg[UO_2^{2+}]$ is calculated as a function of p_{CO_2} at an arbitrarily chosen pH of 4.

Whereas $lg[UO_2^{2+}]$ is constant as a function of lg p_{CO_2} (see eqn. (9)) in equilibrium with $UO_3 \cdot 2H_2O$(s), $lg[UO_2^{2+}]$ in equilibrium with UO_2CO_3(s) decreases with increasing lg p_{CO_2} and, at a partial pressure of 2.8% CO_2, UO_2CO_3(s) becomes the solubility limiting phase up to 100% CO_2 partial pressure. In Fig. 6, the shaded areas take into account the experimental uncertainties of the solubility products. The CO_2 partial pressure, where both phases become unstable with respect to each other, is found between 1.4 and 5.6% with a mean value of 2.8% by eqn. (13)

$$\lg p_{CO_2} = \lg K_{sp}(UO_2CO_3) - \lg K_{sp}(UO_3) + 2 \lg K_w - \Sigma \lg K \quad (13)$$

Equation (13) shows that this point is independent of pH.

TABLE 3. Experimental data on lg K_{22} for $I = 0.1$ M and 25 °C available in the literature

lg K_{22}	Method	Reference
-5.91	pot. titration	3
-5.84	pot. titration	26
-6.09 ± 0.03	pot. titration	27
-6.28 ± 0.02	spectroscopy	27
-5.95 ± 0.04	pot. titration	28
-5.89	pot. titration	29
-5.85 ± 0.30	pot. titration	30
-6.45 ± 0.1	pot. titration	31
-5.97 ± 0.16 (mean)		

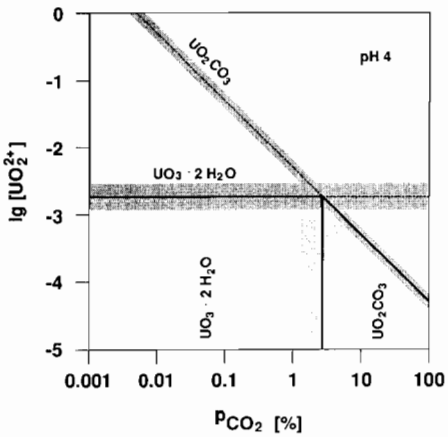

Fig. 6. Calculated $lg[UO_2^{2+}]$ in equilibrium with UO_2CO_3(s) and $UO_3 \cdot 2H_2O$(s), respectively, as function of p_{CO_2}. A phase transition occurs at a partial pressure of 2.8% CO_2. Shaded areas account for uncertainty.

Thermodynamic evaluation

From the present solubility products, Gibbs free energies of reaction according to eqns. (1) and (2), respectively, are calculated to be

$$\Delta G°_R(UO_2CO_3) = +79.28 \pm 0.62 \text{ kJ mol}^{-1}$$

$$\Delta G°_R(UO_3 \cdot 2H_2O) = +127.17 \pm 1.10 \text{ kJ mol}^{-1}$$

Using $\Delta G°_f(UO_2^{2+}{}_{(aq)}) = -952 \pm 2.1$ kJ mol^{-1} [32], calculating $\Delta G°_f(CO_3^{2-}{}_{(aq)})$ from $\Delta G°_f(CO_{2(g)}) = -394.373 \pm 0.140$ [33] and eqn. (5) as $\Delta G°_f(CO_3^{2-}{}_{(aq)}) = -530.94 \pm 0.58$ kJ mol^{-1}, and obtaining $\Delta G°_f(OH^-{}_{(aq)})$ from $\Delta G°_f(H_2O_{(l)}) = -237.140 \pm 0.040$ kJ mol^{-1} [33] and eqn. (3) as $\Delta G°_f(OH^-{}_{(aq)}) = -158.49 \pm 0.10$ kJ mol^{-1}, the following Gibbs free energies of formation of UO_2CO_3(s) (rutherfordine) and $UO_3 \cdot 2H_2O$(s) (schoepite) are calculated

$$\Delta G°_f(UO_2CO_3(s)) = -1562.2 \pm 3.3 \text{ kJ mol}^{-1}$$

$$\Delta G°_f(UO_3 \cdot 2H_2O(s)) = -1633.3 \pm 3.5 \text{ kJ mol}^{-1}$$

These data may be compared to literature values

$$\Delta G°_f(UO_2CO_3(s)) = -1563.1 \text{ kJ mol}^{-1} \text{ [34]}$$

$$\Delta G°_f(UO_3 \cdot 2H_2O(s)) = -1633.4 \text{ kJ mol}^{-1} \text{ [34]}$$

$$\Delta G°_f(UO_3 \cdot 2H_2O(s)) = -1636.8 \pm 1.7 \text{ kJ mol}^{-1} \text{ [35]}$$

Comparison with literature (Table 4)

Our value for lg $K_{sp}(UO_2CO_3)$ is in reasonable agreement with both the data of Sergeeva *et al.* [1] and Grenthe *et al.* [2], considering the differences in the ionic strengths.

TABLE 4. Comparison of present results with experimental data available in the literature

lg K_{sp}	Ionic strength (mol l^{-1})	Conditions	Solid phase	CO_2 partial pressure (%)	Reference
-13.21 ± 0.06	0.5	$NaClO_4$, 25 ± 0.02 °C	UO_2CO_3	4.8–98	2
-13.94 ± 0.06	3.0	$NaClO_4$, 25 ± 0.02 °C	UO_2CO_3	4.8–98	2
−14.26	0.02	$NaHCO_3/HCl/HClO_4$, 25 °C	UO_2CO_3	100	1
-13.89 ± 0.11	0.1	$NaClO_4$, 24 ± 2 °C	UO_2CO_3	100	this work
-21.26 ± 0.02	0.5	$NaClO_4$, 25 °C	$UO_3 \cdot 2H_2O_{(cryst)}$	0 (N_2)[a]	[b]
-20.34 ± 0.01	0.5	$NaClO_4$, 25 °C	$UO_3 \cdot 2H_2O_{(am)}$	0 (N_2)	[c]
−21.74	0.2	NH_4NO_3	$UO_2(OH)_2$		5
−21.96	variable	$NaOH/HClO_4$, 25 °C	$UO_3 \cdot H_2O$	0 (N_2)	6
-21.9 ± 0.3[d]	variable	NH_3/HNO_3	$UO_2(OH)_2$		4
−23.5	0.1	$NaNO_3$	$UO_2(OH)_2$	0 (N_2)	3
-22.20 ± 0.12	0.1	$NaClO_4$, 24 ± 2 °C	$UO_3 \cdot 2H_2O$	0.98	this work
-22.34 ± 0.23	0.1	$NaClO_4$, 24 ± 2 °C	$UO_3 \cdot 2H_2O$	0.03	this work

[a](N_2) = nitrogen atmosphere. [b]Recalculated with lg K_w (0.5 M) = −13.74 [21] from lg K_s = 6.22 [7]. [c]Recalculated with lg K_w (0.5 M) = −13.74 [21] from lg K_s = 6.55 [7]. [d]Data seems to be given for zero ionic strength.

A comparison of the present data for lg $K_{sp}(UO_3 \cdot 2H_2O)$ with literature data is difficult. Most solubility products are given for other solids of unclear physicochemical state without characterization.

Bruno and Sandino [7] have investigated the solubility of schoepite in the pH range 6.7–9 under nitrogen atmosphere. Under those conditions, U(VI) is known to be completely hydrolyzed [36] and the quality of the evaluated solubility product depends completely on the chosen hydrolysis data, the quality of which cannot be verified by the methods used in ref. 7. Available literature data on hydrolysis of U(VI) in the pH region 6.7–9 covers a range of not verified species with discrepancies in the proposed hydrolysis constants for the same aqueous species up to several orders of magnitude [24]. A microcrystalline and an amorphous solid phase is reported in ref. 7, but it is unclear whether the phase $UO_3 \cdot 2H_2O_{(am)}$ is corroborated by the X-ray analysis in the course of the experiment. Hence, the solubility product given in the present work is the only available data on lg $K_{sp}(UO_3 \cdot 2H_2O)$ directly determined on well-characterized schoepite.

Conclusions

UO_2CO_3 (rutherfordine) with lg $K_{sp} = -13.89 \pm 0.11$ in equilibrium with 100% CO_2 partial pressure and $UO_3 \cdot 2H_2O$ (schoepite) with lg $K_{sp} = -22.28 \pm 0.19$ in equilibrium with 0.98 and 0.03% CO_2 partial pressure were characterized by X-ray crystallography, FTIR-PAS, UV–Vis-PAS, DTA/TGA analysis, and solubility studies as solubility limiting solid phases in 0.1 M $NaClO_4$ solutions at 24 ± 2 °C. The phase transition between the two phases was calculated to occur at a CO_2 partial pressure of 2.8%. This is in agreement with the experimental results of Grenthe *et al.* [2], who reported rutherfordine as a solubility limiting solid phase at partial pressures $\geqslant 4.8\%$ CO_2.

The importance of schoepite as a solubility limiting solid phase in natural environments [37] and technical processes [38] has recently been discussed. This study supports this assumption quantitatively. Present data are also in agreement with the occurrence of rutherfordine in natural systems. UO_2CO_3(s) is found to be the stable solid phase above 2.8% CO_2 partial pressures. Natural systems are known to have CO_2 partial pressures up to 10% [8].

Acknowledgements

The authors express their appreciation to Dr Zenko Yoshida and Dr Ole Mogensen for suggestions and discussions.

References

1 E. I. Sergeyeva, A. A. Nikitin, I. L. Khodakhovskiy and G. B. Naumov, *Geochem. Int., 9* (1972) 900.
2 I. Grenthe, D. Ferri, F. Salvatore and G. Riccio, *J. Chem. Soc., Dalton Trans.,* (1984) 2439.
3 K. A. Kraus and F. Nelson, *Rep. AECD-1864,* US Atomic Energy Commission, 1948.
4 R. G. Milkey, *Anal. Chem., 26* (1954) 1800.
5 A. K. Babko and V. S. Kodenskaya, *Russ. J. Inorg. Chem., 5* (1960) 1241.
6 K. H. Gayer and H. Leider, *J. Am. Chem. Soc., 77* (1955) 1448.
7 J. Bruno and A. Sandino, in *Scientific Basis for Radioactive Waste Management XII; Mater. Res. Soc. Symp. Proc., 127* (1989) 871.

8 J. I. Kim, in A. J. Freeman and C. Keller (eds.), *Handbook of the Physics and Chemistry of the Actinides,* Vol. 4, Elsevier, Amsterdam, 1984, Ch. 8, p. 413.
9 W. Runde, G. Meinrath and J. I. Kim, *Radiochim. Acta,* in press.
10 G. Meinrath and H. Takeishi, *J. Alloy Comp.,* in press.
11 T. Kimura, J. Serrano G., S. Nakayama, K. Takahashi and H. Takeishi, *Radiochim. Acta,* in press.
12 *JCPDS Powder Diffraction File,* Table 11-263.
13 *JCPDS Powder Diffraction File,* Table 24-1172.
14 *JCPDS Powder Diffraction File,* Table 29-1376.
15 E. Robinovitch and R. L. Belford, *Spectroscopy and Photochemistry of Uranyl Compounds,* Pergamon, Frankfurt, 1964, p. 20.
16 B. M. Gatehouse, S. E. Livingstone and R. S. Nyholm, *J. Chem. Soc.,* (1958) 3137.
17 H. R. Hoekstra and S. Siegel, *J. Inorg. Nucl. Chem., 18* (1961) 154.
18 J. Weidlein, M. Müller and K. Dehnicke, *Schwingungsspektroskopie,* Thieme, Stuttgart, 1982.
19 G. Socrates, *Infrared Characteristic Group Frequencies,* Wiley–Interscience, New York, 1980.
20 G. Heinrich, H. Güsten and H. J. Ache, *Appl. Spectrosc., 40* (1986) 363.
21 R. Fischer and J. Byé, *Bull. Soc. Chim. Fr.,* (1964) 2920.
22 G. Meinrath and J. I. Kim, *J. Inorg. Solid Chem. Suppl., 28* (1991) 383.
23 W. T. Carnall, in K.-Ch. Buschbeck (ed.), *Gmelin Handbuch der Anorganischen Chemie,* Uran, Vol. 5A, Springer, Berlin, 1982.
24 J. I. Kim, G. Meinrath and V. Neck, Thermodynamic constants of hydrolysis and carbonate complexation of the actinides, *Rep. RCM,* TU München, Inst. f. Radiochemie, to be published.
25 G. R. Choppin and J. N. Mathur, *Radiochim. Acta,* (1991) 25.
26 R. L. Gustafson, C. Richard and A. E. Martell, *J. Am. Chem. Soc., 82* (1960) 1526.
27 M. Bartusek and L. Sommer, *Z. Phys. Chem., 226* (1963) 309.
28 P. A. Overvoll and W. Lund, *Anal. Chim. Acta, 143* (1982) 153.
29 L. Maya, *Inorg. Chem., 21* (1982) 2895.
30 A. Vainiotalo and O. Mäkitie, *Finn. Chem. Lett.,* (1981) 102.
31 M. K. Kotvanova, A. M. Evseev, A. P. Borisova, E. A. Torchenkova and S. V. Zakharov, *Moscow Univ. Chem. Bull., 39* (1984) 37.
32 J. Fuger and F. L. Oetting, *The Chemical Thermodynamics of Actinide Elements and Compounds – II. The Actinide Aqueous Ions,* IAEA, Vienna, 1976, p. 16.
33 D. Gravin, V. B. Parker and H. J. White, Jr. (eds.), *CODATA Thermodynamic Tables,* Springer, Heidelberg, 1987.
34 D. Langmuir, *Geochim. Cosmochim. Acta, 42* (1978) 547.
35 I. R. Tasker, P. A. G. O'Hare, B. M. Lewis, G. K. Johnson and E. H. P. Cordfunke, *Can. J. Chem., 66* (1988) 620.
36 S. Ahrland, in J. I. Katz, G. T. Seaborg and L. R. Morss (eds.), *The Chemistry of the Actinide Elements,* Vol. 2, Chapman and Hall, London, 2nd edn., 1986, p. 1480.
37 K. M. Krupka, D. Rai, R. W. Fulton and R. G. Strickert, in *Scientific Basis for Radioactive Waste Management VIII; Mat. Res. Soc. Symp. Proc., 44* (1985) 753.
38 R. Wey, I. Lauffenburger and D. Saehr, *Bull. Soc. Chim. Fr.,* (1968) 1874.